The Astrophysical Journal, 947:6 (17pp), 2023 April 10 https://doi.org/10.3847/1538-4357/acbb07

Toward Robust Atmospheric Retrieval on Cloudy L Dwarfs: the Impact of Thermal and Abundance Profile Assumptions

Melanie J. Rowland[1], Caroline V. Morley[1], and Michael R. Line[2]
[1] Department of Astronomy, University of Texas at Austin, 2515 Speedway C1400, Austin, TX 78712, USA; mrowland@utexas.edu
[2] School of Earth & Space Exploration, Arizona State University, Tempe, AZ 85287, USA
Received 2022 November 7; revised 2023 January 20; accepted 2023 February 1; published 2023 April 11

Abstract

Constraining L dwarf properties from their spectra is challenging. Near-infrared (NIR) spectra probe a limited range of pressures, while many species condense within their photospheres. Condensation creates two complexities: gas-phase species "rain out" (decreasing in abundances by many orders of magnitude) and clouds form. We designed tests using synthetic data to determine the best approach for retrieving L dwarf spectra, isolating the challenges in the absence of cloud opacity. We conducted atmospheric retrievals on synthetic cloud-free L dwarf spectra derived from the Sonora Bobcat models at SpeX resolution using a variety of thermal and chemical abundance profile parameterizations. For objects hotter than L5 ($T_{\rm eff} \sim 1700$ K), the limited pressure layers probed in the NIR are mostly convective; parameterized pressure–temperature (*PT*) profiles bias results and free, unsmoothed profiles should be used. Only when many layers both above and below the radiative-convective boundary are probed can parameterized profiles provide accurate results. Furthermore, a nonuniform abundance profile for FeH is needed to accurately retrieve bulk properties of early-to-mid L dwarfs. Nonuniform prescriptions for other gases in NIR retrievals may also be warranted near the L/T transition (CH_4) and early Y dwarfs (Na and K). We demonstrate the utility of using realistic, self-consistent models to benchmark retrievals and suggest how they can be used in the future.

Unified Astronomy Thesaurus concepts: Brown dwarfs (185); L dwarfs (894); Atmospheric structure (2309); Atmospheric composition (2120); Stellar atmospheres (1584); Planetary atmospheres (1244)

1. Introduction

Atmospheric studies of brown dwarfs and exoplanets are used to constrain key atmospheric properties that can reveal information about an object's history. The ages of brown dwarfs can be inferred from effective temperatures and surface gravities (Burrows et al. 2001; Saumon & Marley 2008), while metallicities, C/O ratios, and recently carbon isotope ratios have been used to constrain giant planet formation pathways, formation location, and migration (Öberg et al. 2011; Madhusudhan et al. 2014, 2017; Zhang et al. 2021). Brown dwarfs offer the opportunity to study atmospheres with similar chemical complexity to giant planets while removing complications from stellar irradiation and prohibitively low signal-to-noise (S/N).

Inferring the bulk properties of brown dwarfs and exoplanets has been done by comparing the object's near-infrared (NIR) spectrum to model spectra generated from theoretical models (Cushing et al. 2008). One of the two prevailing modeling techniques is self-consistent models computed on grids of effective temperature and surface gravity. Early brown dwarf models assumed radiative-convective thermochemical equilibrium and were either adapted from solar system models for hotter and more massive objects (Marley et al. 1996) or from cool star models for cooler and less massive objects (Burrows et al. 1993). These models have evolved in complexity to include clouds (Ackerman & Marley 2001), rainout of gases (Lodders & Fegley 2002; Marley et al. 2021), and disequilibrium chemistry (Phillips et al. 2020; Mukherjee et al. 2022; Lacy & Burrows 2023), and rely on assumed atmospheric chemistry paradigms and one-dimensional radiative-convective equilibrium (Burrows et al. 2001; Marley & Robinson 2015) to reduce the dimensionality of the models.

The inclusion of more complex atmospheric processes in grid models has resulted in improved data–model agreement and granted key insights into the chemical and physical phenomena at play. However, the nature of grid modeling limits inferences regarding object properties to only those specified as grid dimensions. Remaining data–model mismatches across all existing grid models imply that some assumptions required by grid modeling may not be valid in many objects.

Atmospheric retrievals provide better data–model fits and determination of atmospheric properties not included in grid models. The better model fits come from relaxing some of the assumptions that are needed in self-consistent models and replacing them with many parameters that are directly determined. These better data–model fits come with several risks. The larger number of parameters can lead to overfitting, and the relaxation of parameters can lead to unphysical results, so retrieval parameterization and interpretation require careful consideration. Two important parameterization choices include the thermal profile and the chemistry.

1.1. Thermal Profile Parameterization in Retrievals

Thermal profile parameterizations must allow some degree of flexibility while producing physically realistic profiles. Less complex and less flexible profiles make more assumptions about the structure of the atmosphere, but require fewer parameters, which may be warranted for low-S/N or low-

resolution observations. Profiles used in retrievals include a five-parameter joint exponential power law (Madhusudhan & Seager 2009; Burningham et al. 2017), a six-parameter radiative-convective power law with flexible upper atmospheres (Gravity Collaboration et al. 2020; Mollière et al. 2020), a variable-parameter (two–∞) piece-wise polynomial profile (Kitzmann et al. 2020), and a 17-parameter free profile (Line et al. 2015).

1.2. Chemistry Parameterization in Retrievals

Similarly, the chemistry parameterization has fallen into two categories: equilibrium chemistry and "free" chemistry. Most equilibrium-chemistry retrievals typically only retrieve the bulk metallicity and the C/O ratio and then use the thermal profile to obtain abundance profiles by either interpolating from a precomputed equilibrium-chemistry grid or calculating them directly using an equilibrium-chemistry code like `FastChem` (Stock et al. 2018). The latter method allows changing element abundances instead of assuming solar ratios. This type of parameterization is useful when only a few model parameters are justified due to sparse or low-S/N spectra, such as in Mollière et al. (2020), but its ability to accurately characterize atmospheres relies heavily on model assumptions, as in grid models. In general, hot atmospheres tend to relax into a state of chemical equilibrium because the chemical timescale is short at high temperatures. Departures from chemical equilibrium can be incorporated with quench pressure approximations and rainout condensation can be incorporated into equilibrium-chemistry grids, but conclusions about chemical abundances and gas ratios different from solar ratios are still limited. Alternatively, the free-chemistry approach directly retrieves abundances for a determined subset of gases, in which the abundance profile of each trace species is retrieved independently by one constant with altitude (or "uniform") parameter per species. Changeat et al. (2019) and Bourrier et al. (2020) employed nonuniform approaches, but required five or four parameters for a nonuniform gas, respectively. The flexibility of free-chemistry approaches allows retrievals to characterize more molecular and atomic ratios, while the drawbacks include a large number of parameters, retrieving nonphysical abundances, and not capturing nonuniform with pressure abundance profiles that may be important when rainout chemistry impacts prominent opacity sources.

1.3. Prior Brown Dwarf Retrieval Results

The increased flexibility provided by these thermal and chemistry profile parameterizations have allowed retrievals to identify regimes where grid model assumptions break down and to identify missing model physics. Free-chemistry retrievals allow carbon, nitrogen, and oxygen reservoir gases as well as alkalis to vary independently, in contrast to grid models that require abundances change in concert to maintain chemical equilibrium. Line et al. (2017) and Zalesky et al. (2019) showed that retrieved abundances in mid-T dwarfs can largely be explained by chemical equilibrium, but retrievals in the late L dwarf regime by Burningham et al. (2017) indicate that either chemical disequilibrium via vertical mixing or nonsolar CNO ratios are needed to explain retrieved abundances. Line et al. (2017) and Zalesky et al. (2019) also showed decreasing alkali abundances starting in objects with $T_{\rm eff} = 1000$ K through the late T and early Y dwarf sequence. This indicated a departure from pure local thermochemical equilibrium models, which predicted decreasing alkali abundances by 1200 K, and instead favored rainout chemistry as predicted by Lodders (1999) and Burrows et al. (2001).

1.4. The Challenges of L Dwarf Retrievals

Flexible thermal profile retrievals have shown that radiative-convective equilibrium is valid in T and Y dwarfs (Line et al. 2015, 2017; Kitzmann et al. 2020; Zalesky et al. 2022). However, many retrieval studies of L dwarfs have favored isothermal temperature profiles (Burningham et al. 2017; Lueber et al. 2022; Gonzales et al. 2022). Multiple explanations for this preferred profile have been suggested. One explanation is the presence of clouds, which add gray opacity at the observed NIR wavelengths. These clouds mimic an isothermal profile and obscure flux from deeper layers. Tremblin et al. (2016) suggests an alternative to the L dwarf cloud paradigm to explain the isothermal profiles by invoking an adiabatic index lowered by thermochemical convection arising from the transition from CO/CH_4 in an out-of-equilibrium atmosphere.

These open questions surrounding L dwarf properties highlight the difficulty in expanding retrieval frameworks to hotter temperatures. While these thermal and abundance profile parameterizations have been successful at retrieving cloud-free late T benchmarks like Gl-570D (Line et al. 2015; Burningham et al. 2017; Kitzmann et al. 2020) and retrieving most bulk properties up the T dwarf sequence (Line et al. 2017; Lueber et al. 2022; Zalesky et al. 2022) and down the Y dwarf sequence (Zalesky et al. 2019), the validity of these parameterizations and their effects on retrieved bulk properties have not been robustly tested at hotter temperatures.

Three main challenges exist in NIR modeling of L dwarfs. (i) NIR opacity windows that probe many layers of the atmosphere in cooler objects close with the rise of hydride and oxide opacities; the NIR spectra of L dwarfs probe only a narrow range of the atmosphere, which inhibits robust thermal profile characterization. (ii) Prominent opacity sources at cooler temperatures are expected to have uniform with pressure abundance profiles, while prominent absorbers at hotter temperatures like hydrides and oxides are heavily impacted by rainout, making their abundance profiles strongly nonuniform. (iii) The presence of clouds increasingly impacts mid-to-late L dwarf spectra and complicates analyses because they are degenerate with an isothermal profile and obscure atmospheric structure below the cloud layers.

In light of these challenges, we aim to assess whether our existing thermal and chemical profile parameterizations are adequate in retrieving accurate bulk properties. In this paper, we tackle two of the three challenges. First, which pressure–temperature (*PT*) profile parameterizations accurately retrieve bulk properties and thermal profiles with spectral information from limited pressure ranges? Second, what kind of free-chemistry profile parameterizations accurately retrieve bulk properties in objects with abundances that are strongly nonuniform?

To do this, we perform a suite of retrievals using a variety of thermal and abundance parameterizations on synthetic benchmarks generated from self-consistent grid model spectra for which we know ground-truth properties. While real mid-to-late L dwarfs are expected to have clouds, we retrieve on cloud-free

Table 1
Molecular Opacity Sources

Species	Source
H_2O	Tennyson & Yurchenko (2018), Barber et al. (2006)
CH_4	Yurchenko et al. (2013), Yurchenko & Tennyson (2014)
CO	H10[a]; Li et al. (2015)
CO_2	Huang et al. (2014)
NH_3	Yurchenko et al. (2011)
PH_3	Sousa-Silva et al. (2015)[b]
TiO	Schwenke (1998), Allard et al. (2000)
VO	McKemmish et al. (2016); ExoMol[b]
MgH	Weck et al. (2003)[c]
CrH	Burrows et al. (2002)
FeH	Dulick et al. (2003), Hargreaves et al. (2010)

Notes.
[a] HT10 = HITEMP 2010 (Rothman et al. 2010): http://www.cfa.harvard.edu/hitran/HITEMP.html.
[b] http://www.exomol.com (Tennyson & Yurchenko 2012).
[c] http://www.physast.uga.edu/ugamop/.

synthetic spectra to isolate the effects the other two challenges pose to our retrieval parameterizations. In Section 2.1, we detail how we generate the synthetic benchmarks, and in Section 2.2 we detail the retrieval framework and the tested thermal and chemistry parameterizations. In Section 3 we show results and the winning parameterizations. Finally, in Section 4 we discuss how this informs the validity of model assumptions in different regimes.

2. Methods

Retrieving on synthetic spectra we generate ourselves allows us to know ground-truth values of not only bulk properties like effective temperature, surface gravity, metallicity, and C/O ratios, but also the true thermal profile and abundance profiles, something that is not possible with real benchmark objects. We describe our synthetic spectra in Section 2.1 and the suite of retrievals with varying parameterizations we performed on them in Section 2.2.

2.1. Data

The CHIMERA retrieval framework's forward model was used to create two synthetic ∼L2 spectra based on the self-consistent cloud-free Sonora Bobcat model's $T_{\rm eff} = 2000$ K, $\log(g) = 5.0$, solar metallicity, solar C/O object (Marley et al. 2021) at 10 pc. Both spectra use the Sonora model's *PT* profile (91 layers, $\log(P) = -3.75$–1.643 bars) and 14 selected gas species. The gas species included are H_2O, CO, CO_2, CH_4, NH_3, Na, K, PH_3, TiO, VO, FeH, CrH, MgH, and H^-, along with H_2–H_2 and H_2–He collision-induced absorption opacities. We use the absorption cross-section sources from the Marley et al. (2021) Sonora Bobcat models for these 14 gases and provide the molecular cross-section sources in Table 1.

The first L2 spectrum was designed to isolate the effects of narrow pressure ranges probed due to increased hydride and oxide opacity at high temperatures. This spectrum was generated with uniform with pressure chemistry profiles for the 14 gas species. Self-consistent chemistry profiles from the Sonora models were analyzed and mixing ratios for each gas were held constant at their value at 1 bar, corresponding to the values in the middle of the photosphere. This uniform chemistry spectrum was used to test different *PT* profile parameterizations and to inform the parameterizations of subsequent retrievals. In addition to this L2, $T_{\rm eff} = 2000$ K spectrum, we also generated two additional uniform chemistry spectra (L5, $T_{\rm eff} = 1700$ K and L7, $T_{\rm eff} = 1600$ K) using the same approach to explore the effects of *PT* profile parameterizations across multiple spectral types.

The second L2 spectrum was designed to include the effects of nonuniform chemistry profiles, which are expected to occur with rainout chemistry. Mixing ratios for each gas were determined by the self-consistent chemistry profiles from the Sonora model. This self-consistent chemistry spectrum was used to test different free-chemistry parameterizations.

The output spectra were binned to Infrared Telescope Facility SpeX (0.95–2.5 μm, $R \approx 120$) resolution. All SpeX Prism Library (Burgasser 2014) L and T dwarfs with $R \approx 120$ and S/N > 25 were analyzed, mean errors bars at each wavelength were calculated and added to the spectra, and each data point was sampled from a normal distribution characterized by the binned spectral point and error bar at each wavelength to add synthetic noise. The two L2 synthetic data sets and the chemistry profiles used to generate each are shown in Figure 1.

2.2. Retrieval Framework

We adapted the CHIMERA retrieval framework (Line et al. 2015) for retrieval of hot ($T_{\rm eff} = 2000$ K) synthetic spectra. We tested four different thermal profile parameterizations and two different chemistry abundance profile parameterizations, with the number of total free parameters ranging from 20 to 36 depending on model parameterization. All models used the radiative-transfer core described in Zalesky et al. (2022), which adapted Lacis & Oinas (1991) for use on graphics processing units (GPUs). We utilized the Anaconda Numba `guvectorize` framework on NVIDIA Quadro RTX 5000 GPUs on Frontera at the Texas Advanced Computing Center. The GPU memory (16 GB) limited the number of simultaneous CPU threads to four; however, Frontera hosts four GPUs per computing node, which enabled four separate retrievals to be run concurrently.

All retrievals included the same 14 species (H_2O, CO, CO_2, CH_4, NH_3, Na, K, PH_3, TiO, VO, FeH, CrH, MgH, and H^-) and H_2–H_2 and H_2–He collision-induced absorption opacities used to create the synthetic data. Cross sections were sampled at a constant $R = 12{,}500$ for SpeX resolution ($R = 120$), similar to Line et al. (2015) and Zalesky et al. (2019, 2022).

Parameter estimation for all retrievals was conducted using the `emcee` package (Foreman-Mackey et al. 2013), as in the previously mentioned studies. All retrievals were run out to 60,000 iterations with 224–272 walkers depending on the number of free parameters. The highest and lowest number of parameter models were run out to 120,000 iterations with no significant difference in retrieved posteriors. Initial guesses were constructed by a "Gaussian ball" centered on a by-eye fit for each parameter, and solutions were insensitive to initial guesses. Parameters for all tested retrieval models along with their priors are provided in Table 2.

2.2.1. Tested Thermal Profiles

The thermal profile refers to how the temperature varies with pressure in the atmosphere. In this work, four different thermal profile parameterizations were tested to determine

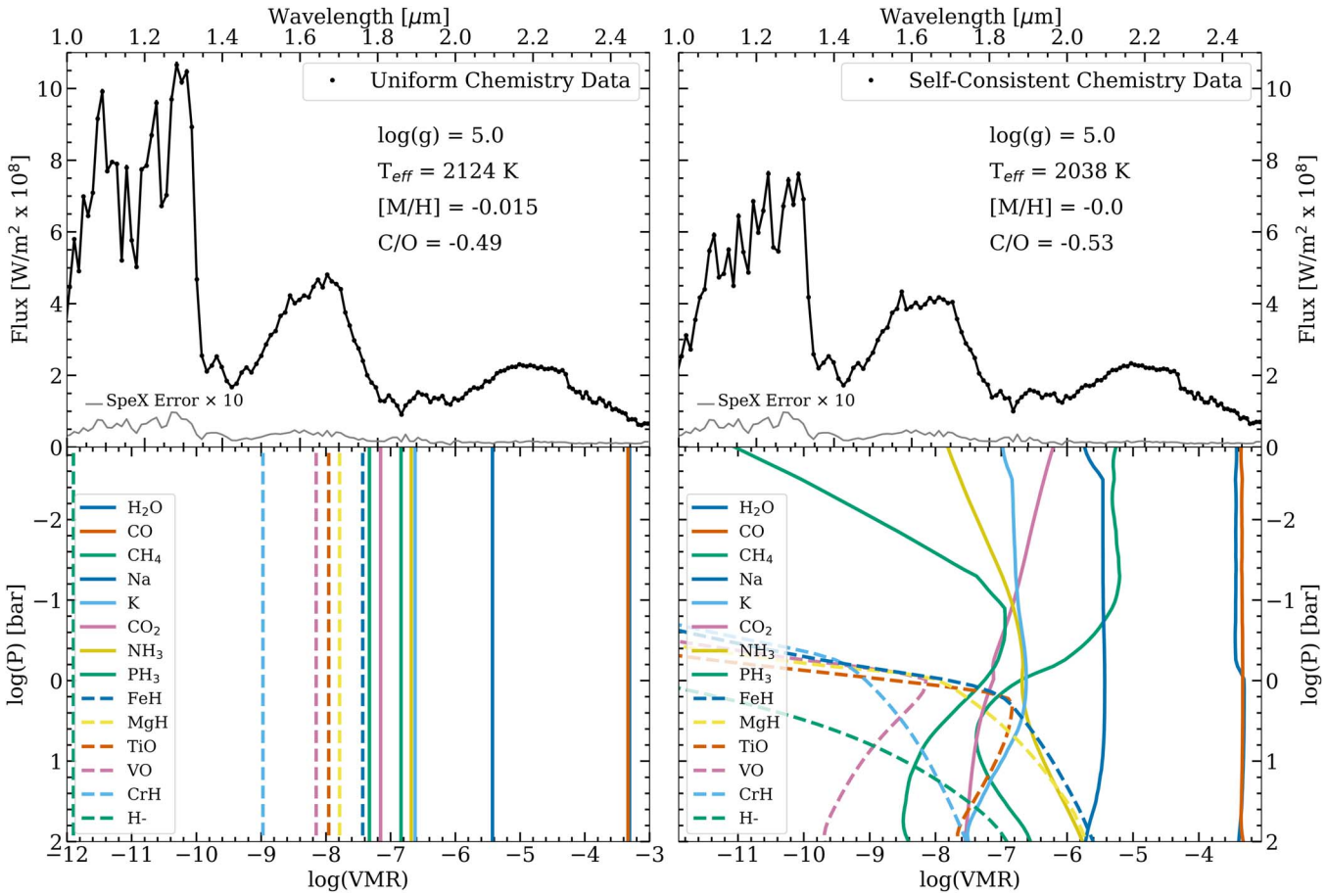

Figure 1. L2 ($T_{\rm eff} = 2000$ K) synthetic spectra (top) generated with uniform chemistry (left) or self-consistent chemistry (right) in black with characteristic SpeX error × 10 in gray for visibility. The chemistry profiles for the 14 gas species used to generate each spectrum are shown in the bottom panels.

Table 2
Retrieved Parameters

Parameter	Description	Prior
$\log(g)$	Log of surface gravity (cm s^{-2})	<6, M <1 00 M_J
$(R/D)^2$	Radius-to-distance scale factor (R_J/pc)	<1, M < 100 M_J
10[b]	Error bar inflation	0.01 × min (σ_i^2), 100 × max (σ_i^2)
T_i[a]	Temperature (K) at a given pressure level	<5500 K
γ, β[b]	Smoothing hyperparameters (Equation (5); Line et al. 2015)	Inv. Gamma ($\Gamma(\gamma, \alpha, \beta)$), $\alpha = 1$
$T_{\rm app}$[c]	Approximate temperature (K)	<4000 K
$\log(\bar{\kappa})$[c]	Log of mean opacity	>−5, <1.5
RCB[c]	Radiative-convective boundary layer (bars)	>0.01, <30 bars
γ_p[d]	Nongrayness	>1, <100
$\log(\tau_{\rm lim})$[d]	Extent of nongrayness	>−4, <1
$\log(f_i)$	Log of VMR of a uniform gas	>−12, $\sum f_i = 1$
BL$_j$[e]	Boundary layer (bars) for a nonuniform gas	>0.001, <315 bars
$\log(a_j)$[e]	Log of VMR of a nonuniform gas below BL$_j$	>−12, $\sum (f_i+a_j) = 1$
$\log(b_j)$[e]	Log of VMR of a nonuniform gas above BL$_j$	>−12, $\sum (f_i+b_j) = 1$

Notes.
[a] Smoothed and unsmoothed *PT* retrievals only.
[b] Smoothed *PT* retrievals only.
[c] Gray and nongray RC *PT* retrievals only.
[d] Nongray RC *PT* retrievals only.
[e] Nonuniform gas retrievals only.

the accuracy with which each captures the ground-truth *PT* profile and ground-truth bulk properties. Each of these parameterizations are tested on the uniform chemistry spectrum.

1. *"Unsmoothed" free.* The most flexible thermal profile is the free-unsmoothed profile (henceforth "unsmoothed" *PT* profile), which is parameterized by 15 temperature variables equidistant in $\log(P)$ space between −3.5 and

2.5. This 15-point profile is connected by Hermite spline interpolation and is then interpolated onto the finer 70-point pressure grid for the radiative-transfer calculation. There is no smoothing, which can allow for unphysical oscillations from layer to layer.

2. *"Smoothed" free.* The next most flexible profile is the free-smoothed profile ("smoothed" *PT* profile) from Line et al. (2015), which is parameterized as above, but with the addition of two smoothing hyperparameters that penalize the second derivative of the profile. This profile allows oscillations if there is sufficient evidence to justify curvature of the profile. This profile becomes less adequate as the probed pressure layers narrow for hotter objects.
3. *"Gray RC."* We constructed a third radiative-convective profile characterized by a gray radiative upper atmosphere and a convective adiabat lower atmosphere ("gray RC" profile). This profile is parameterized by four parameters. The gray radiative portion from Guillot (2010) is constructed by surface gravity ($\log(g)$) and mean opacity ($\log(\bar{\kappa})$) parameters to control the optical depth to pressure mapping and an approximate temperature parameter ($T_{\rm app}$) to set the Eddington approximation gray radiative profile, as described in Equation (1):

$$T^4(\tau) = \frac{3T_{\rm app}^4}{4}\left(\frac{2}{3} + \tau\right). \quad (1)$$

The final parameter is the location of the radiative-convective boundary (RCB) in bars. The convective part of the atmosphere is set by a dry adiabat as described in Robinson & Catling (2012) and characterized by the temperature and pressure at the boundary and is set by $\frac{\partial \ln T}{\partial \ln P}$ of the final two radiative layers. The RCB can vary within the prior because the *PT* profile is parameterized independently from the chemistry, unlike Mollière et al. (2020) where the RCB and convective adiabat are determined by the equilibrium-chemistry grid.

4. *"Nongray RC."* The gray radiative profile from Guillot (2010) causes an isothermal upper atmosphere that is hotter than the thermal profiles from the self-consistent Sonora models. We constructed a fourth *PT* profile to incorporate the nongray effects in the upper atmosphere ("nongray RC" profile). We use the nonirradiated, nongray parameterization from Chandrasekhar (1935) as described by Equation (28) in Parmentier & Guillot (2014) below:

$$T^4(\tau) = \frac{3T_{\rm app}^4}{4}\left(\tau + \frac{\frac{2}{3} + \sqrt{\frac{1}{3\gamma_P}}}{1 + \frac{1}{2}\sqrt{3\gamma_P}}\right) + \frac{3T_{\rm app}^4}{4}\left(\frac{\gamma_P - 1}{\sqrt{\gamma_P}}\right)\frac{\frac{1}{\sqrt{3}} + \sqrt{\gamma_P}\tau_{\rm lim}}{1 + \frac{1}{2}\sqrt{3\gamma_P}}(1 - e^{\frac{-\tau}{\tau_{\rm lim}}}). \quad (2)$$

This profile is constructed with six parameters: $\log(g)$, $\log(\bar{\kappa})$, $T_{\rm int}$, the RCB, $\tau_{\rm lim}$, and γ_P. The lower atmosphere is characterized by a convective adiabat as described above, but the upper atmosphere is constrained by Equation (2), where γ_P controls the nongrayness of the upper atmosphere and $\tau_{\rm lim}$ controls the optical depth to which the nongrayness extends in the atmosphere. Like the gray radiative-convective profile, this profile is also parameterized independently from the chemistry.

Table 3
Retrieval Tests

Data	*PT* Profile	Nonuniform Gas	Parameters
Uniform	Gray RC	None	20
Uniform	Nongray RC	None	22
Uniform	Unsmoothed	None	32
Uniform	Smoothed	None	34
Self-consistent	Gray RC	None	20
Self-consistent	Nongray RC	None	22
Self-consistent	Unsmoothed	None	32
Self-consistent	Smoothed	None	34
Self-consistent	Unsmoothed	FeH	34
Self-consistent	Unsmoothed	K	34
Self-consistent	Unsmoothed	H_2O	34
Self-consistent	Unsmoothed	VO	34
Self-consistent	Unsmoothed	CrH	34
Self-consistent	Unsmoothed	CO	34
Self-consistent	Unsmoothed	TiO	34
Self-consistent	Unsmoothed	Na	34
Self-consistent	Unsmoothed	FeH+K	36

2.2.2. Tested Chemical Abundance Profiles

The chemical abundance profiles of all included opacity species throughout the atmosphere are described by volume mixing ratios (VMRs). We tested two free-chemistry models.

The first chemical abundance profile parameterization tested was the existing free-chemistry model, which used uniform with pressure profiles for all 14 gases (H_2O, CO, CO_2, CH_4, NH_3, Na, K, PH_3, TiO, VO, FeH, CrH, MgH, and H^-) retrieved. The chemistry in these models was controlled by 14 mixing ratios, one for each gas. This provided the flexibility to retrieve disequilibrium species but did not allow species to vary throughout the atmosphere. This parameterization was used in all retrievals on the uniform chemistry spectrum and also tested on the self-consistent chemistry spectrum.

The second type of chemical profile tested was a step function, where the abundance profile for a single gas was controlled by three parameters: an upper mixing ratio, a lower mixing ratio, and a pressure layer where the abundance changed ("nonuniform" profile). For these retrievals, we set all profiles as uniform with the exception of one gas (and later two gases), which had the nonuniform profile. The chemistry in these models was controlled by 16 parameters (13 uniform profiles and one nonuniform profile). This chemistry parameterization was tested on the self-consistent chemistry spectrum.

A detailed description of each retrieval test performed including the spectrum retrieved on, the thermal profile parameterization, the chemistry parameterization, and the total number of parameters is provided in Table 3.

3. Results

In this section we present results from the retrieval tests. Comparisons of retrieved thermal profiles, abundance profiles, and bulk properties are presented. While some properties like surface gravity, radius, and abundance profiles are retrieved directly, other bulk properties like *PT* profiles, effective temperatures, metallicity, and C/O are derived based on

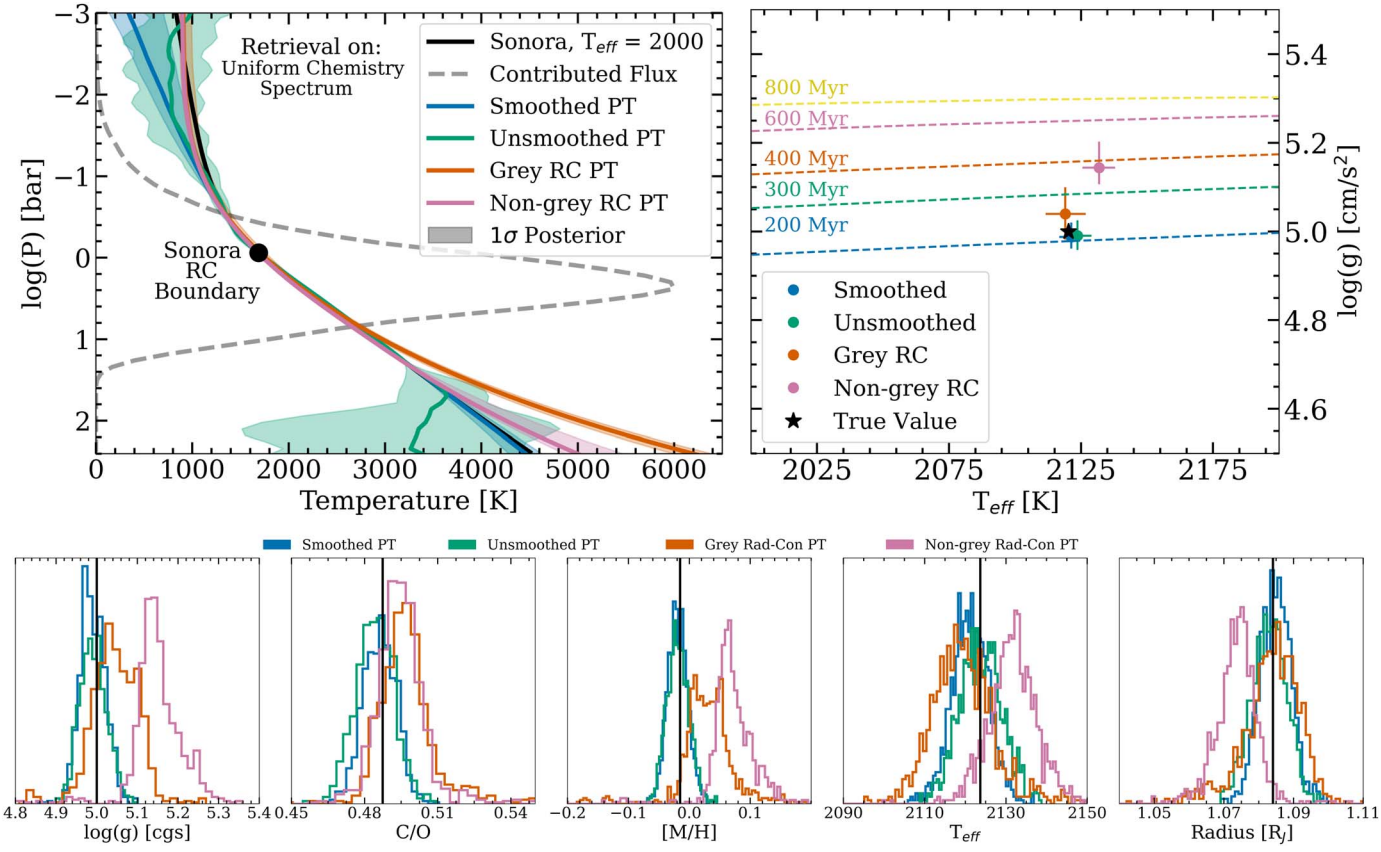

Figure 2. Retrieved *PT* profiles, bulk properties, and inferred ages using four *PT* profile parameterizations (colors), ground-truth Sonora values (black), and isochrones from Marley et al. (2021; dashed colors). Retrievals done on the uniform chemistry spectrum. The free thermal profiles accurately retrieve bulk properties but do not reliably constrain the upper atmosphere.

retrieved parameters. The derivations of each of these parameters are described below.

Free (smoothed and unsmoothed) *PT* profiles are constructed by using Hermite spline interpolation between the 15 directly retrieved temperature points. Radiative-convective profiles are constructed using the retrieved parameters and Equations (1) or (2). As in Line et al. (2017), Zalesky et al. (2019), and Zalesky et al. (2022), effective temperature is derived by equating Boltzmann's law to the bolometric fluxes between 0.7 and 20 μm derived from 1000 model spectra drawn from the posterior.

Metallicity is computed as

$$[\mathrm{M/H}] = \log\left(\frac{(\mathrm{M/H})_{\mathrm{retrieved}}}{(\mathrm{M/H})_{\mathrm{solar}}}\right), \quad (3)$$

where the retrieved metallicity is taken to be the summation of the elemental species included in the retrieval model. The C/O ratio is computed as

$$\frac{\mathrm{C}}{\mathrm{O}} = \frac{\sum \mathrm{C}}{\sum \mathrm{O}} \approx \frac{\mathrm{CH_4} + \mathrm{CO} + \mathrm{CO_2}}{\mathrm{H_2O} + \mathrm{CO} + 2\mathrm{CO_2} + \mathrm{VO} + \mathrm{TiO}}. \quad (4)$$

More complex thermal and chemistry profile parameterizations use more parameters but may provide a better fit to the data. The Bayesian information criterion (BIC) was computed for all retrievals to determine if the inclusion of additional parameters resulted in better fits to the data. The BIC was calculated as

$$\mathrm{BIC} = -2\ln(L) + \ln(N)\mathrm{K}, \quad (5)$$

where $\ln(L)$ is the log-likelihood of the best-fit model, N is the number of data points, and K is the number of parameters. The model with the lowest BIC signals the better model. As in Kass & Raftery (1995) and Gonzales et al. (2021), we use the following intervals for selecting between two models with evidence against the higher BIC as $0 < \Delta\mathrm{BIC} < 2$: no preference worth mentioning; $2 < \Delta\mathrm{BIC} < 6$: positive; $6 < \Delta\mathrm{BIC} < 10$: strong; and $10 < \Delta\mathrm{BIC}$: very strong.

3.1. Thermal Profile Retrievals

All *PT* profile parameterizations were tested on the uniform chemistry spectrum. Figure 2 shows the median and 1σ *PT* profiles retrieved by each model compared to the ground-truth Sonora *PT* profile for the L2 object. The bottom figure shows the bulk properties retrieved or derived by each model compared to the ground-truth Sonora bulk properties. Also shown are the inferred ages based on retrieved surface gravity and effective temperature. Table 4 shows the bulk properties retrieved or derived for the four *PT* profiles tested. Bolded values indicate disagreement with the ground-truth values. Appendix A shows all retrieved chemical abundances for the four *PT* parameterizations. Only the smoothed and unsmoothed *PT* profiles accurately retrieve all abundances and bulk properties from the uniform chemistry spectrum.

NIR SpeX resolution spectra for objects of this type probe a narrow pressure range, as shown by the gray dashed line in Figure 2. The pressures probed contain mostly a linear part of the temperature profile, so a more linear *PT* profile is preferred

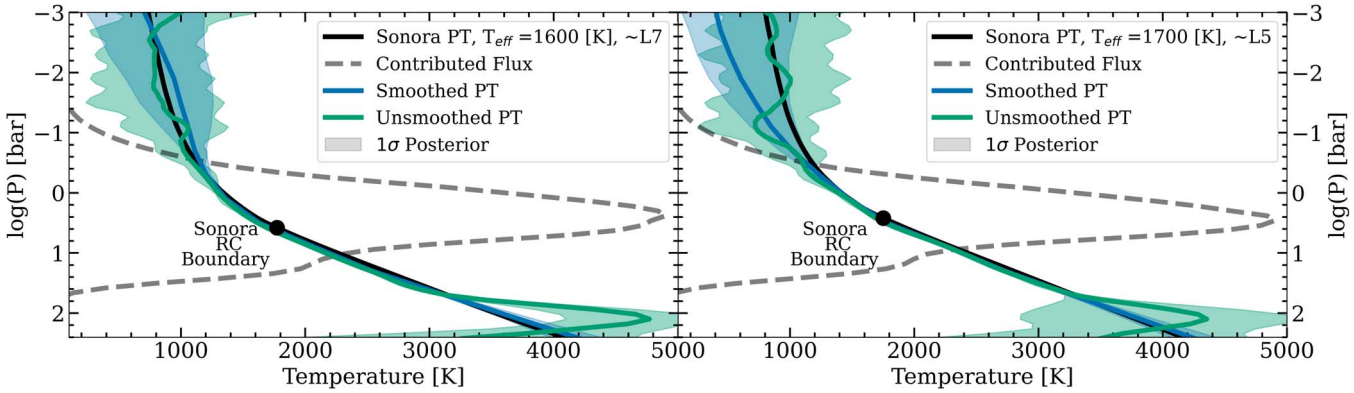

Figure 3. Retrieved thermal profiles for two synthetic L dwarfs showing that a smoothed *PT* profile can accurately retrieve the thermal profile of objects later than L6, but retrieves a cooler upper atmosphere for objects earlier than L5.

Table 4
Thermal Profile Retrieval Results

Data	*PT* Profile	log(g)	Radius	Mass	$T_{\rm eff}$	[M/H]	C/O	ΔBIC
Uniform	Sonora	5.0	1.084	47.4	2124	−0.015	0.487	N/A
Uniform	Gray RC	5.04 ± 0.06	1.09 ± 0.01	52^{+7}_{-6}	2119^{+8}_{-7}	$0.03^{+0.05}_{-0.03}$	0.50 ± 0.01	−16
Uniform	Nongray RC	$5.14^{+0.06}_{-0.04}$	1.07 ± 0.01	65^{+9}_{-5}	2132 ± 6	$0.07^{+0.04}_{-0.02}$	0.49 ± 0.01	−8
Uniform	Unsmoothed	$4.99^{+0.03}_{-0.04}$	1.08 ± 0.01	46^{+4}_{-3}	2124 ± 5	-0.02 ± 0.02	0.48 ± 0.01	···
Uniform	Smoothed	4.98 ± 0.03	1.09 ± 0.01	46 ± 3	2121 ± 4	-0.02 ± 0.02	0.49 ± 0.01	−172
Self-consistent	Sonora	5.0	1.084	47.4	2038	0.00	0.534	N/A
Self-consistent	Gray RC	5.27 ± 0.03	$1.13^{+0.02}_{-0.07}$	96^{+3}_{-7}	1987^{+70}_{-25}	$0.49^{+0.50}_{-0.25}$	$0.65^{+0.04}_{-0.06}$	−23
Self-consistent	Nongray RC	$5.25^{+0.05}_{-0.43}$	1.11 ± 0.03	88^{+8}_{-57}	2007^{+29}_{-23}	$0.19^{+0.23}_{-0.11}$	$0.59^{+0.04}_{-0.06}$	−13
Self-consistent	Unsmoothed	$5.20^{+0.08}_{-0.09}$	1.08 ± 0.02	75^{+14}_{-13}	2038^{+18}_{-20}	$0.16^{+0.12}_{-0.07}$	$0.56^{+0.04}_{-0.05}$	···
Self-consistent	Smoothed	$5.25^{+0.04}_{-0.11}$	1.11 ± 0.02	90^{+8}_{-17}	2007^{+23}_{-24}	$0.17^{+0.12}_{-0.10}$	$0.59^{+0.04}_{-0.06}$	−219

in a smoothed parameterization. The unsmoothed *PT* profile is only constrained in this probed region. Neither the gray RC nor the nongray RC parameterizations converge on an RC boundary. Table 4 shows that neither the smoothed nor unsmoothed *PT* profiles bias retrieved bulk properties, but Figure 2 shows that a smoothed *PT* profile retrieves a colder profile above the photosphere while an unsmoothed *PT* profile retrieves unphysical oscillations above and below the photosphere for an ~L2 object with $T_{\rm eff} = 2000$ K.

3.1.1. Thermal Profile Retrievals on Different Spectral Types

We conducted additional retrievals on uniform chemistry data for an ~L5 object with $T_{\rm eff} = 1700$ K and an ~L7 object with $T_{\rm eff} = 1600$ K to determine for which spectral type a retrieved smoothed *PT* profile can no longer be trusted above the photosphere. We retrieved both objects with a smoothed and unsmoothed *PT* profile parameterization, and the retrieved *PT* profiles can be seen in Figure 3. The smoothed *PT* profile retrieves an accurate profile for L6 objects and later but a cooler upper atmosphere for objects earlier than L5.

3.2. Thermal Profile Retrievals on the Self-consistent Chemistry Spectrum

Most brown dwarf retrievals assume uniform with altitude abundance (Burningham et al. 2017; Line et al. 2017; Zalesky et al. 2019); we mimicked this approach for our synthetic data by retrieving on the self-consistent chemistry spectrum with all four *PT* profile parameterizations assuming uniform chemistry parameterizations. The retrieved *PT* profiles, bulk properties, and inferred ages are shown in Figure 4, and the bulk properties retrieved and derived are shown in Table 4. The smoothed, unsmoothed, gray, and nongray radiative-convective profiles do not agree with the Sonora *PT* profile, and almost all retrieved or derived bulk properties and ages for all *PT* parameterizations are in disagreement at the 1σ level. Appendix A shows the retrieved abundances for all four *PT* parameterizations. All four models retrieve a higher CO abundance than the input profile, and all models except the unsmoothed model retrieve higher CO_2 and H^- abundances. For this spectral type, no choice of *PT* profile can accurately retrieve values in this regime if uniform chemistry is used.

3.3. Chemical Abundance Profile Retrievals

All retrievals testing different abundance profile parameterizations were conducted on the self-consistent chemistry spectrum, which used both the Sonora *PT* profile and abundance profiles. All retrievals used the unsmoothed *PT* profile parameterization, which provided the most unbiased results in Section 3.1.

We include one fully uniform abundance retrieval in which all 14 gases had uniform (constant with altitude) abundances, and eight retrievals in which 13 gases had uniform abundances and one gas had the nonuniform abundance parameterization (step function). The six gases that were not tested for nonuniform profiles were the gases for which only upper limits were retrieved in the retrievals on the uniform chemistry

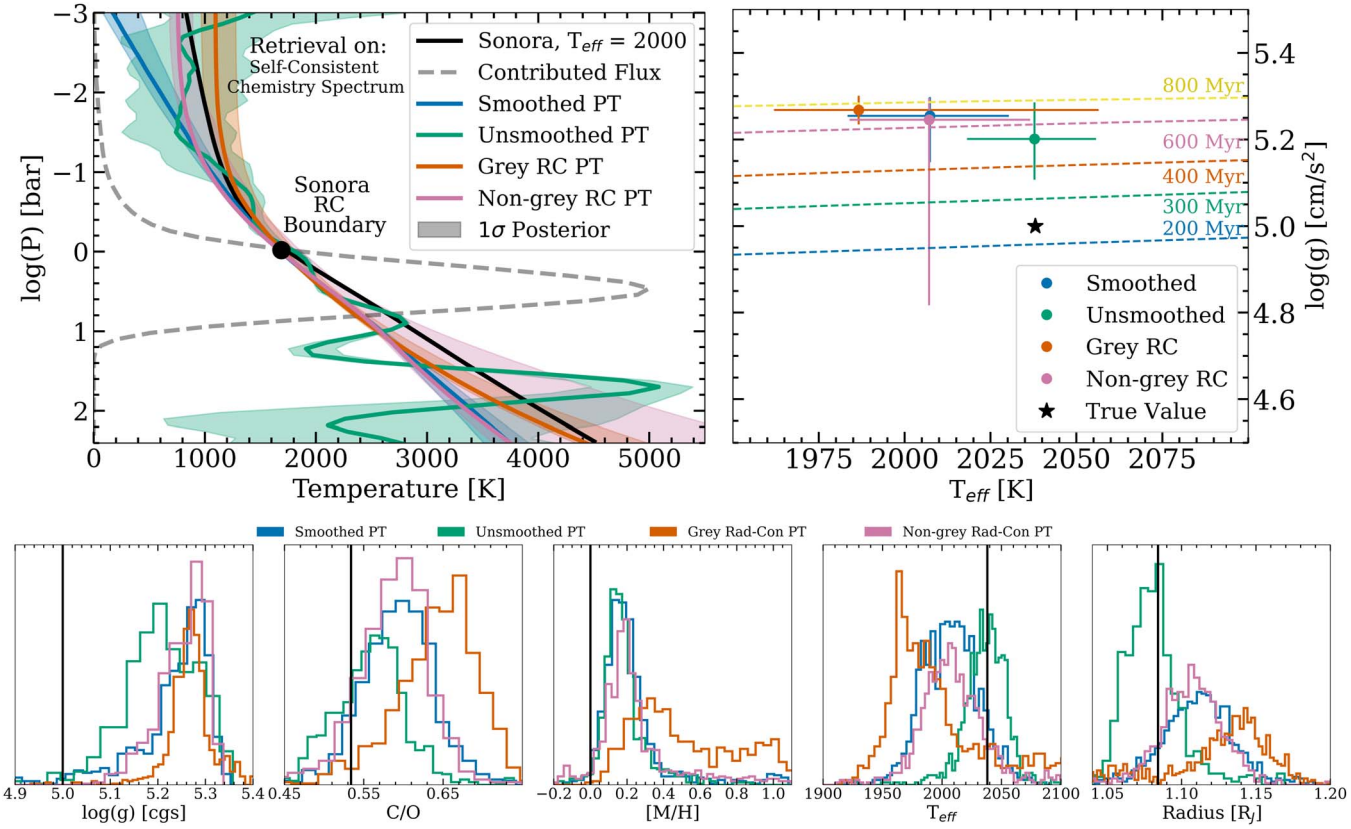

Figure 4. Same as Figure 2 but for retrievals done with the self-consistent chemistry spectrum. Thermal profiles, bulk properties, and inferred ages are inaccurately retrieved regardless of *PT* profile parameterization.

Table 5
Self-consistent Chemistry Retrieval Results

Data	Nonuniform Gas	log(g)	Radius	Mass	$T_{\rm eff}$	[M/H]	C/O	ΔBIC
Self-consistent	Sonora	5.0	1.084	47.4	2038	0.00	0.534	N/A
Self-consistent	None	$5.20^{+0.08}_{-0.09}$	1.08 ± 0.02	75^{+14}_{-13}	2038^{+18}_{-20}	$0.16^{+0.12}_{-0.07}$	$0.56^{+0.04}_{-0.05}$	⋯
Self-consistent	FeH	$5.06^{+0.05}_{-0.06}$	1.08 ± 0.01	54^{+6}_{-7}	2040 ± 7	0.013 ± 0.03	0.53 ± 0.01	289
Self-consistent	K	$5.24^{+0.06}_{-0.09}$	$1.08^{+0.02}_{-0.01}$	81^{+10}_{-13}	2039^{+14}_{-15}	$-0.30^{+0.19}_{-0.09}$	$0.15^{+0.04}_{-0.09}$	35
Self-consistent	H_2O	$5.03^{+0.15}_{-0.35}$	$1.10^{+0.03}_{-0.02}$	53^{+19}_{-28}	2021^{+23}_{-29}	$0.22^{+0.25}_{-0.18}$	$0.33^{+0.11}_{-0.13}$	35
Self-consistent	VO	$5.19^{+0.09}_{-0.12}$	1.08 ± 0.02	73 ± 17	2034^{+17}_{-19}	$0.09^{+0.11}_{-0.10}$	0.56 ± 0.04	5.7
Self-consistent	CrH	$5.22^{+0.08}_{-0.09}$	$1.08^{+0.2}_{-0.1}$	77^{+13}_{-14}	2039^{+16}_{-17}	$0.11^{+0.11}_{-0.08}$	0.56 ± 0.04	3.7
Self-consistent	CO	5.21 ± 0.08	1.08 ± 0.02	76^{+14}_{-11}	2039^{+15}_{-18}	$-0.07^{+0.28}_{-0.30}$	$0.34^{+0.25}_{-0.30}$	0.56
Self-consistent	TiO	$5.21^{+0.08}_{-0.11}$	1.08 ± 0.02	77 ± 14	2039^{+13}_{-22}	$0.10^{+0.11}_{-0.08}$	0.56 ± 0.04	−0.48
Self-consistent	Na	$5.19^{+0.09}_{-0.11}$	$1.08^{+0.02}_{-0.01}$	74 ± 15	2037^{+15}_{-20}	$0.09^{+0.09}_{-0.10}$	0.56 ± 0.04	−3.1
Self-consistent	FeH + K	5.02 ± 0.07	1.08 ± 0.09	50^{+8}_{-7}	2034^{+8}_{-9}	-0.06 ± 0.03	0.54 ± 0.02	279

spectrum, indicating that not enough information in the spectrum exists to justify a more complex treatment. An additional retrieval with both nonuniform FeH and K was also performed.

Inclusion of a nonuniform gas in the retrieval adds an additional two parameters to the model (secondary abundance and boundary pressure). Retrieved and derived bulk properties for all 10 retrievals are shown in Table 5. We only retrieve accurate bulk properties when nonuniform FeH is included. The nonuniform FeH retrieval was strongly preferred over a fully uniform retrieval (ΔBIC = 289) and was also strongly preferred over every other retrieval.

The two most preferred nonuniform gas retrievals were FeH (ΔBIC = 289) and K (ΔBIC = 35). An additional retrieval with both nonuniform FeH and nonuniform K was strongly preferred over the uniform chemistry model (ΔBIC = 279), but was not preferred over nonuniform FeH alone (ΔBIC = −11), indicating that adding additional nonuniform gases beyond FeH was not justified.

The retrieved *PT* profiles of the fiducial fully uniform chemistry retrieval and the winning nonuniform FeH retrieval are shown in Figure 5. The only retrieval in which the *PT* profile is retrieved accurately through the photosphere is the nonuniform FeH retrieval. While a uniform chemistry retrieval was able to accurately retrieve the *PT* profile in the photosphere of the uniform chemistry spectrum (Figure 2), it fails on the self-consistent chemistry spectrum. The retrieved profile shows many nonphysical oscillations. In particular, the cooler than expected oscillation at $\log(P) = 1.2$ and the warmer than expected oscillation at $\log(P) = 1.8$ also appear in all retrievals

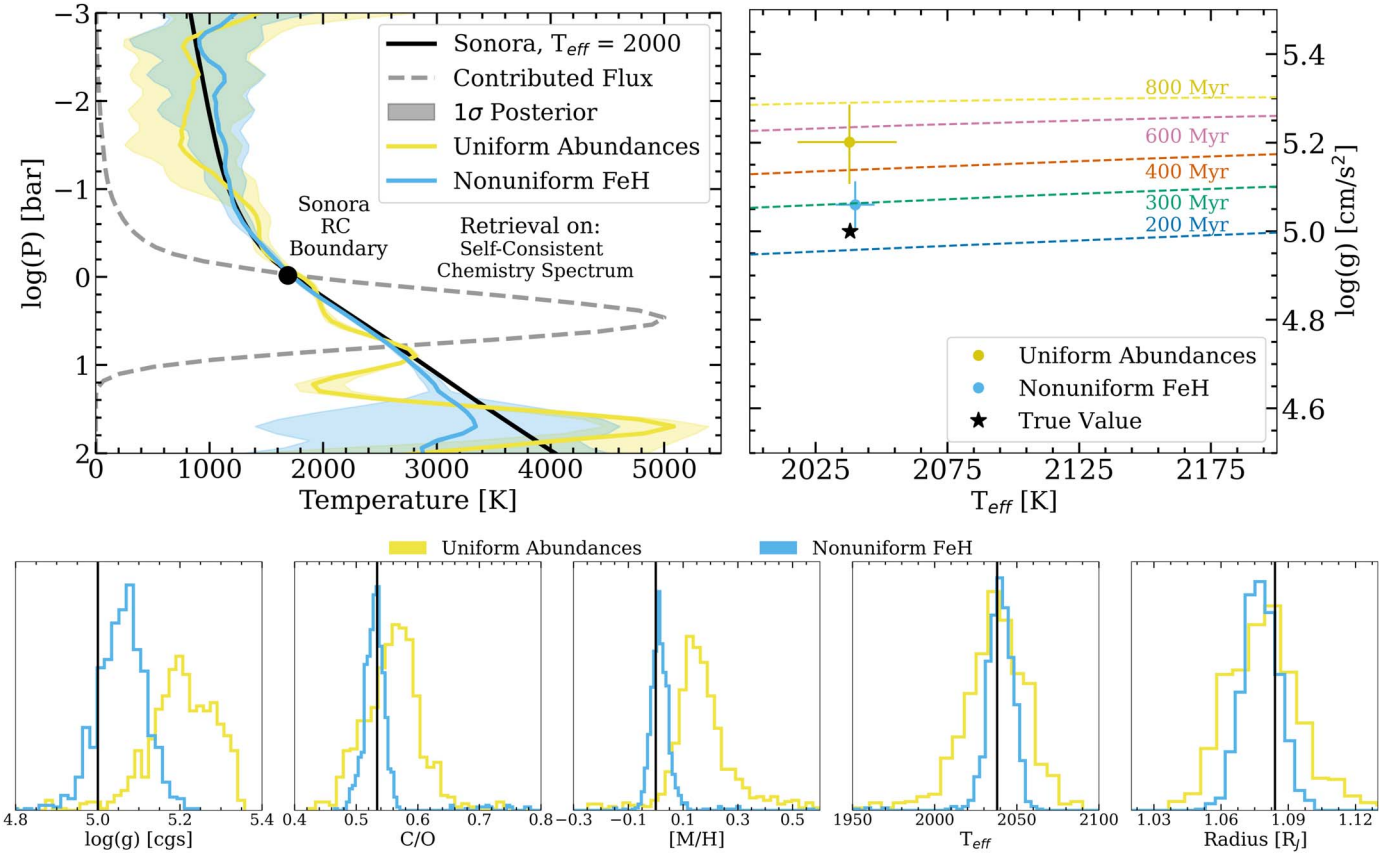

Figure 5. Retrieved *PT* profiles, bulk properties, and inferred ages using two different free-chemistry parameterizations (colors), ground-truth Sonora values (black), and isochrones from Marley et al. (2021; dashed colors). Accurate bulk properties are only retrieved by including a nonuniform abundance profile for FeH.

that have uniform FeH parameterizations, regardless of the other nonuniform gases.

Figure 5 also shows the retrieved or derived bulk properties including surface gravity, radius, C/O ratio, metallicity, and effective temperature, along with inferred ages and isochrones from Marley et al. (2021). The fully uniform free-chemistry retrieval biased retrieved surface gravity, mass, and metallicity. The age inferred from surface gravity and effective temperature was not in agreement with the ground-truth value at the 1σ level.

The retrieved chemistry abundance profiles from the winning nonuniform FeH retrieval is shown in Figure 6. Only the six most abundant gases are shown, and all gases except FeH have uniform retrieved abundances. The Sonora abundance profiles for prominent species like CO, H_2O, Na, and K have relatively uniform abundances that are closely matched by the uniform parameterization. TiO has a strongly nonuniform profile, and the retrieved uniform abundance matches the expected abundance through the photosphere (shaded gray). The FeH abundance profile (deep blue) is a step function that tracks the expected abundances of more FeH in the lower atmosphere followed by swift removal from the atmosphere around 1 bar due to rainout. All retrieved abundances for this retrieval are shown in Appendix A. The corner plot and retrieved spectra are provided in Appendix B.

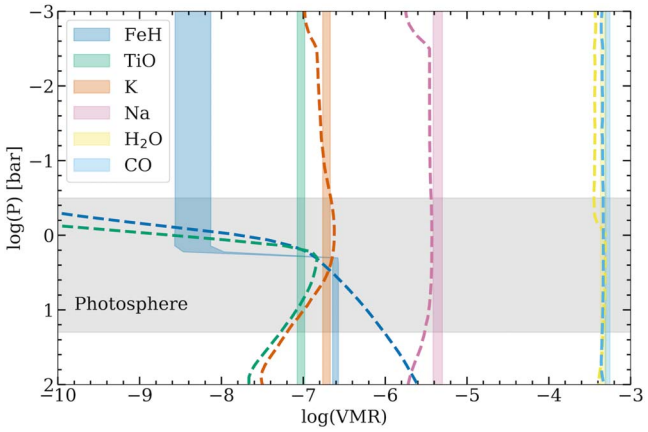

Figure 6. Sonora (dashed) and 1σ retrieved (shaded) abundance profiles of the six most abundant species with the photosphere shaded in gray. All gas species except for FeH are retrieved as uniform with pressure. FeH is retrieved as a step function that accurately retrieves rainout information.

4. Discussion

We performed retrievals on synthetic L dwarf spectra for which we know all ground-truth values in order to answer two questions. First, which *PT* profile parameterizations accurately retrieve bulk properties and thermal profiles with spectral information from limited pressure ranges? Second, what kind of free-chemistry profile parameterizations accurately retrieve bulk properties in objects with abundances that are strongly nonuniform? In this section we discuss the answers to these questions and provide additional analyses that aim to inform future L dwarf retrievals.

4.1. Constraining Thermal Profiles in L Dwarf Atmospheres

We find that the "smoothed free" *PT* profile prescriptions used in prior brown dwarf retrieval models (Line et al. 2015) do

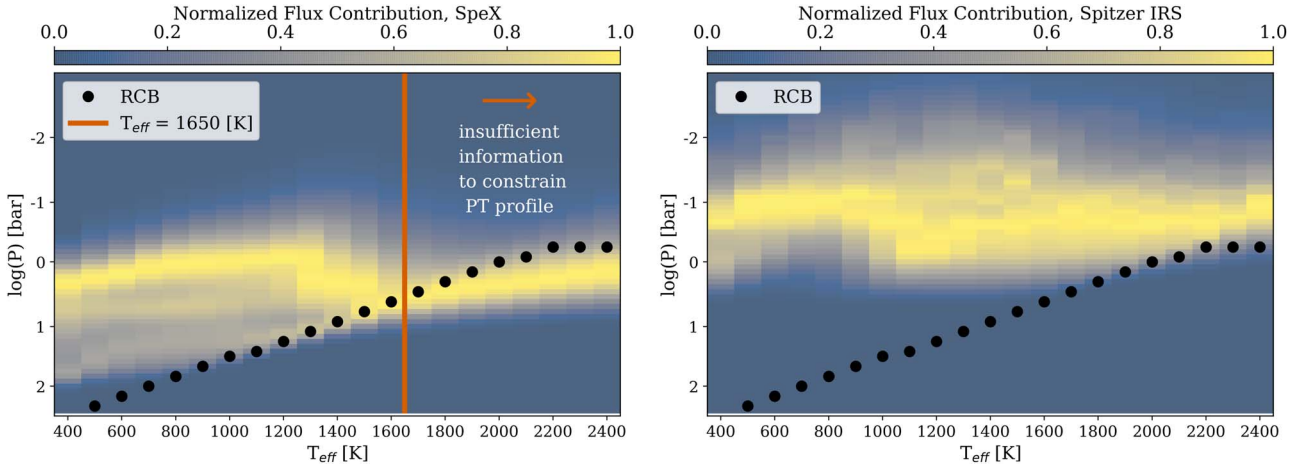

Figure 7. The RCB from cloud-free Sonora models for objects with $T_{\rm eff} = 500$–2400 K. Shading indicates SpeX ($\lambda = 1.0$–2.5 μm, $R \approx 120$) (left) normalized contributed flux from each layer. Fewer layers are probed at hotter temperatures, which makes thermal profile characterization difficult for NIR spectra. The same plot for the Spitzer InfraRed Spectrograph (IRS; $\lambda = 5.2$–14 μm, $R \approx 90$) coverage (right) showing additional layers probed with extended wavelength coverage.

not successfully reproduce the upper atmospheres of early L dwarfs: the parameters that prioritize smoothness end up creating a linear *PT* profile that is cooler than the true profile for objects above ∼1700 K. Here we explain the physical reason for this, and provide a rule-of-thumb for future L dwarf retrievals.

Thermal profile characterization of these hotter objects is difficult because of the number and location of pressure layers probed with NIR spectra. Radiative-convective profiles have a characteristic change in slope at the boundary between the convective layers (which are steeper) and the radiative layers (which are more isothermal). This RCB rises to higher altitudes for hotter objects; for objects warmer than about 1700 K, NIR spectra probe mostly the convective regions of the atmosphere. Because they do not adequately capture the curvature at the RCB, all *PT* profile parameterizations will struggle to reproduce that structure robustly.

Figure 7 shows the RCB from the cloud-free Sonora models with $T_{\rm eff} = 500$–2400 K and shading indicating the normalized contributed flux at each layer from SpeX ($\lambda = 1.0$–2.5 μm, $R \approx 120$) spectra. Fewer layers are probed at hotter temperatures even in the absence of clouds. The orange line in Figure 7 indicates where the smoothed *PT* profile parameterization started to retrieve cooler-than-expected upper atmospheres (similarly, an unsmoothed *PT* profile was unconstrained outside of the probed pressure layers, though still captured the true *PT* profile within the 1σ uncertainties). The narrow range of pressures probed in the L2 spectrum also impacted more structured *PT* profiles like the gray and nongray RC profiles, which retrieved hotter profiles deep in the atmosphere and resulted in incorrect retrieved abundances, metallicities, and surface gravities.

The right plot of Figure 7 shows the same information but for the Spitzer InfraRed Spectrograph (IRS; $\lambda = 5.2$–14 μm, $R \approx 90$) coverage. The mid-infrared (MIR) spectra probe lower pressures since the opacities of species generally increase from NIR to MIR wavelengths; the pressures probed are located in the radiative part of the atmosphere. We therefore find that combining NIR and MIR data of early-to-mid L dwarfs probes convective regions (in the NIR) and radiative regions (in the MIR), giving the retrieval information about the *PT* profile curvature.

This agrees with previous retrievals of 2M2224-0158, a cloudy L4.5 dwarf. Burningham et al. (2017) were unable to retrieve a PT profile with SpeX NIR data alone, but Burningham et al. (2021) were able to constrain both the *PT* profile and some cloud properties when combining NIR and MIR SpeX, Infrared Camera and Spectrograph L band, and Spitzer IRS data for the object. While we successfully constrained bulk properties like surface gravity, effective temperature, metallicity, and C/O ratios with only NIR data, MIR data is needed to robustly determine the thermal profile and cloud properties for early-to-mid L dwarfs.

Our rule-of-thumb for future retrievals is as follows: for an object with the estimated $T_{\rm eff}$/log g of the target, use a self-consistent model to understand whether observations probe both above and below the RCB. If observations only probe the deep convective atmosphere, proceed with caution with parameterized *PT* profiles and do not trust the retrieved thermal profile above the RC boundary.

4.2. "Free" Chemistry Approaches in Brown Dwarfs

When conducting retrieval tests on the cloud-free L2 self-consistent chemistry spectrum, ignoring the effects of rainout chemistry and strongly nonuniform abundances resulted in skewed surface gravities, metallicities, C/O ratios, and incorrect *PT* profiles.

We determined that a nonuniform (step function) FeH profile resulted in accurate bulk properties and photospheric thermal profiles. This best-fit model retrieved uniform abundances for all species except FeH and was strongly preferred over all other free-chemistry parameterizations.

Nonuniform FeH chemistry is needed to accurately retrieve abundances in this object because FeH is both a strong absorber in the NIR and is heavily affected by rainout chemistry. In this section, we expand the analysis to predict at what temperatures other species are likely to have both strongly nonuniform abundances and a significant impact on NIR spectra; these are the species most likely to warrant including nonuniform abundances in retrievals.

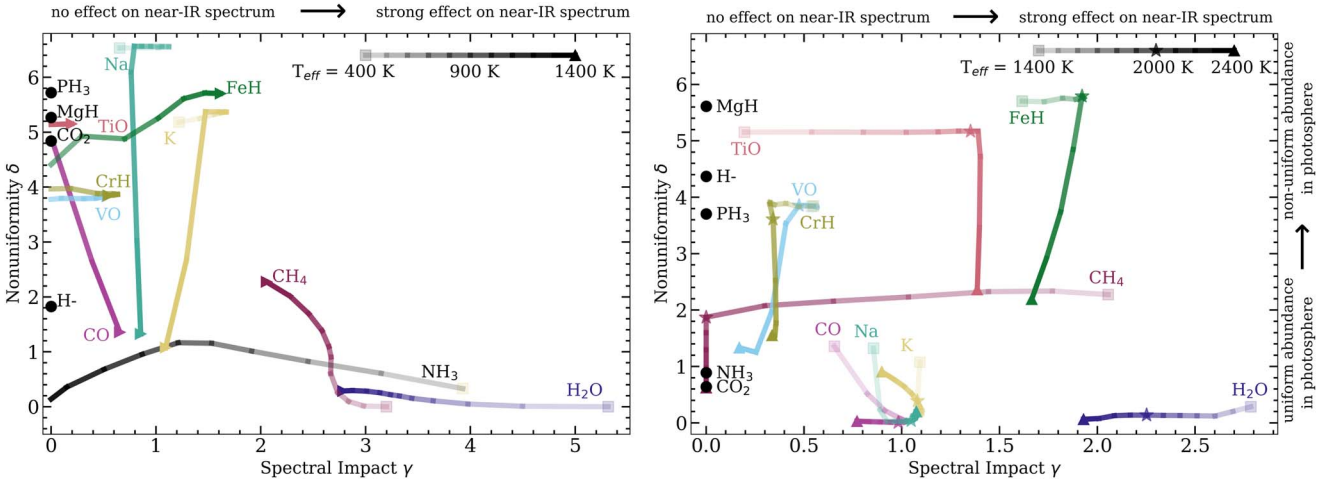

Figure 8. Nonuniformity vs. spectral impact of 14 gases for T and Y dwarfs (left) and L dwarfs (right). Color gradients indicate different effective temperatures. Gases in the upper right of each plot have high spectral impact and have highly nonuniform abundance profiles. Gases whose removal does not impact any data points in the spectrum above the noise are indicated with black circles. The stars on the right plot indicate the values for the 2000 K object studied in this paper.

4.2.1. Applicability of Nonuniform Chemistry

A more complex abundance profile for a given gas would only be warranted if the gas both strongly impacts the observed spectrum and is expected to be strongly nonuniform in the atmosphere. We defined both a "nonuniformity index" and a "spectral impact index" to determine which gases may warrant a more complex abundance profile in objects with a range of effective temperatures.

Nonuniformity, δ, was determined by the change in mixing ratio of the gas in the photosphere using Equation (6):

$$\delta = \max(\log_{10} f_i) - \min(\log_{10} f_i), \quad (6)$$

where f_i is the VMR of a gas abundance profile at level i in the atmosphere. We restrict the atmospheric layers considered to the photosphere, which is determined by the contributed flux in each layer of the atmosphere. We impose a lower limit of $\min(\log_{10} f_i) = -12$.

The spectral impact, γ, is determined by comparing the Sonora spectrum for the object to the spectrum with the gas removed using Equation (7):

$$\gamma = \log_{10} \max\left(\frac{F_{\text{gas},i} - F_{\text{Sonora},i}}{F_{\text{Sonora},i}}\right) + 1.52, \quad (7)$$

where $F_{\text{gas},i}$ is the flux from the spectrum with a gas removed at wavelength i and $F_{\text{Sonora},i}$ is the flux from the Sonora spectrum at wavelength i for SpeX data ($R = 120$, $\lambda = 1.0$–2.5 μm). The values were shifted by 1.52 so that a value of 0 aligns with a spectral impact less than the mean spectral noise. Appendix C shows the effect of varying the abundance of each gas for a $T_{\text{eff}} = 2000$ K spectrum and can be used to inform gases included in future retrievals. Small changes (± 0.3 dex) in gases like H_2O and FeH have large impacts on the spectrum, while large changes (± 2.0 dex) in gases like CO_2 and H^- have no effect on the spectrum.

We used the Sonora spectra at NIR SpeX resolution and the Sonora abundance profiles to calculate these indices for the 14 gas species in this paper in 21 objects with T_{eff} ranging from 400 to 2400 K ($\log(g) = 5.0$, solar metallicity and C/O), and the results are displayed in Figure 8. The gases for the object studied in this paper ($T_{\text{eff}} = 2000$ K) are indicated by stars in the right plot.

A nonuniform FeH abundance profile was needed to accurately retrieve bulk properties for a 2000 K object. Figure 8 shows that FeH has high nonuniformity and high spectral impact between 1800 and 2200 K, but becomes more uniform at hotter temperatures as rainout occurs above the photosphere. This holds true for all species with prominent rainout features above 2200 K. Zalesky et al. (2019) found that alkalis are affected by rainout in late T and early Y spectra. Similarly, we find that alkalis have high nonuninformity and relatively high spectral impact in early Y spectra ($T_{\text{eff}} \approx 600$ K). A simpler two-parameter nonuniform profile (deep atmosphere abundance and cutoff pressure) might be considered for species that are expected to undergo total depletion via rainout. Additionally, CH_4 has high spectral impact starting with late L dwarfs. While not affected by rainout, its abundance profile can vary by more than two orders of magnitude in the photosphere. Therefore, these gases may warrant nonuniform abundance profiles in future retrieval work.

Figure 8 is only applicable for low-resolution NIR data, and would change depending on wavelength coverage and resolution. Deviations from chemical equilibrium and solar abundances would also change values. Oxide (particularly TiO) abundances are expected to have strongly nonuniform profiles due to rainout near the photosphere in objects as cool as 1400 K; however, their features are most strongly seen in the optical.

Our rule-of-thumb for future retrievals is that practitioners should use self-consistent models to guide their analysis: any spectrally active gases likely to vary by more than two orders of magnitude in abundance within the photosphere should warrant additional tests to see if a nonuniform abundance should be used.

5. Conclusions

Characterizing L dwarfs is challenging due to their narrow NIR photospheres, the rainout of prominent opacity sources, and the presence of clouds. This work sought to inform future retrievals by addressing the first two of these challenges. We conducted atmospheric retrievals on synthetic cloud-free L dwarf SpeX spectra derived from the Sonora Bobcat models.

We tested a variety of *PT* profile and abundance profile parameterizations to determine how they bias retrieved bulk properties such as surface gravity, effective temperature, metallicity, and C/O ratios.

1. For early L dwarfs, parameterized *PT* profiles retrieved biased results for most bulk properties. Free, unsmoothed *PT* profiles accurately retrieved all bulk properties.
2. Both NIR and MIR data are needed to constrain *PT* profiles in early-to-mid L dwarfs because NIR data alone probes mostly convective regions of their atmospheres, below the RCB.
3. For atmospheres with nonuniform species, assuming that all gases have uniform abundances causes the retrieved gravity, metallicity, and C/O ratios to be incorrect, regardless of *PT* profile parameterization. A nonuniform (step function) abundance profile for FeH was needed to accurately retrieve bulk properties for an L2 dwarf.
4. Nonuniform FeH is needed for early-to-mid L dwarf NIR retrievals. Other rainout species like TiO may need nonuniform treatment at optical wavelengths. Nonuniform prescriptions may also be important near the L/T transition (CH_4) and early Y dwarfs (Na and K) with the same spectral coverage.

We have demonstrated the utility of using self-consistent models to guide retrievals. We used sophisticated self-consistent models to assess the validity of retrieval techniques for L dwarfs, finding several shortcomings of prior approaches. We presented two rules-of-thumb for practitioners. First, consider the location of the RCB compared to the pressures probed by observations; aim to collect data that probes both radiative and convective layers to constrain the key curvature of the profile, and be cautious when applying parameterized *PT* profiles without this. Second, consider spectrally active gases likely to vary by more than two orders of magnitude in abundance in the photosphere, and include tests to assess nonuniformity. Future retrievals should also consider doing tests such as those presented here using self-consistent models rather than toy models, to be sure that their approach is unbiased and can capture the complexity of real substellar atmospheres.

The authors acknowledge the Texas Advanced Computing Center (TACC) at The University of Texas at Austin for providing high-performance computing resources that have contributed to the research results reported within this paper. URL: http://www.tacc.utexas.edu. M.J.R. acknowledges funding from NASA FINESST grant No. 80NSSC20K1550. C.V.M. acknowledges funding from National Science Foundation AAG grant No. 1910969.

Software: CHIMERA (Line et al. 2013), `emcee` (Foreman-Mackey et al. 2013), `corner.py` (Foreman-Mackey 2016).

Appendix A
Retrieved Abundances

This appendix contains posterior distributions for the included gas phase abundances for all retrievals performed on the L2 spectra. Figure 9 displays results for the retrieval performed on the uniform chemistry spectrum and Figure 10 displays results for the retrieval on the self-consistent chemistry spectrum.

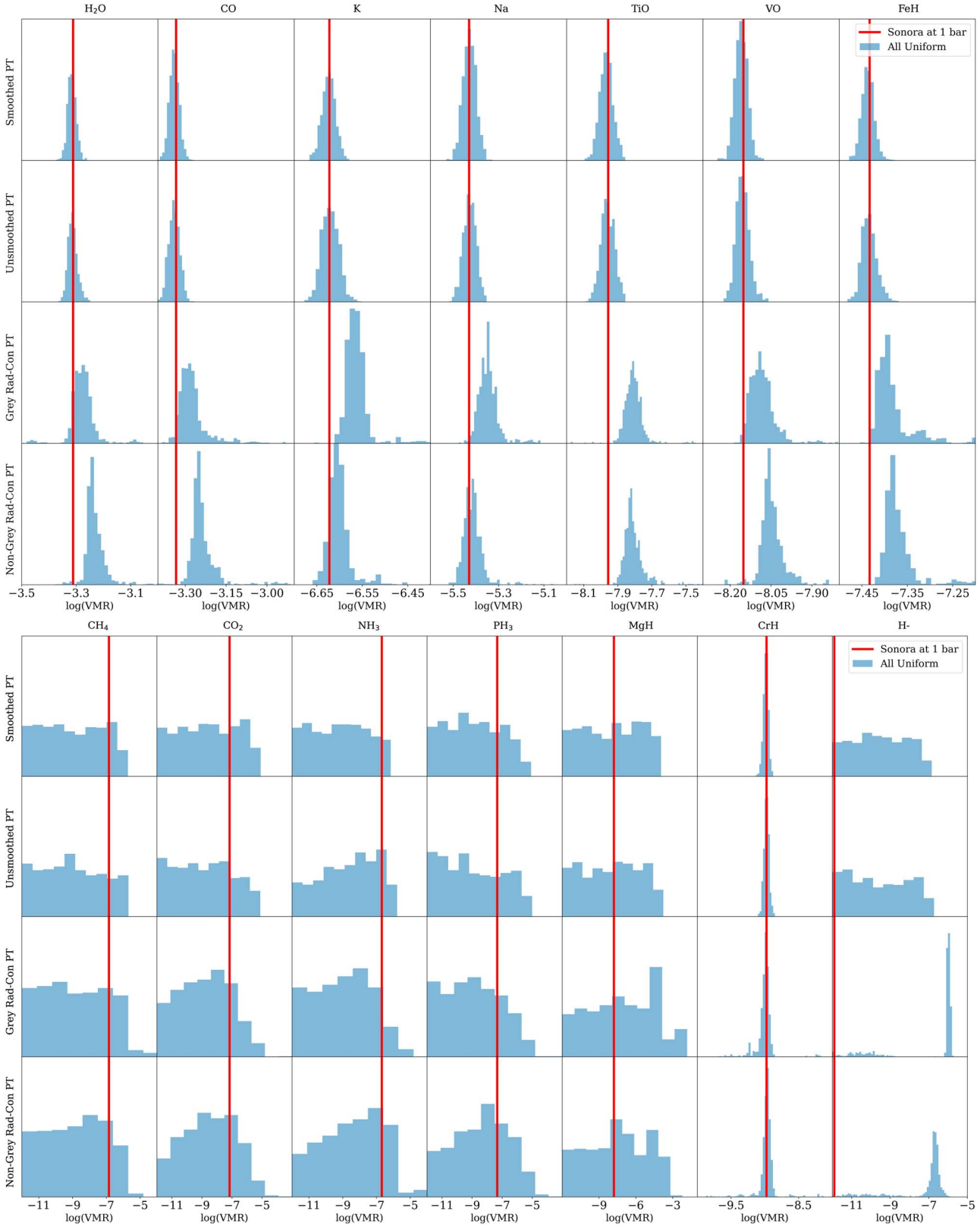

Figure 9. The posteriors of the uniform abundance parameters (blue) and the input uniform chemistry profiles (red) for the four thermal profiles tested. The top plot shows constrained species and the bottom plot shows mostly unconstrained species.

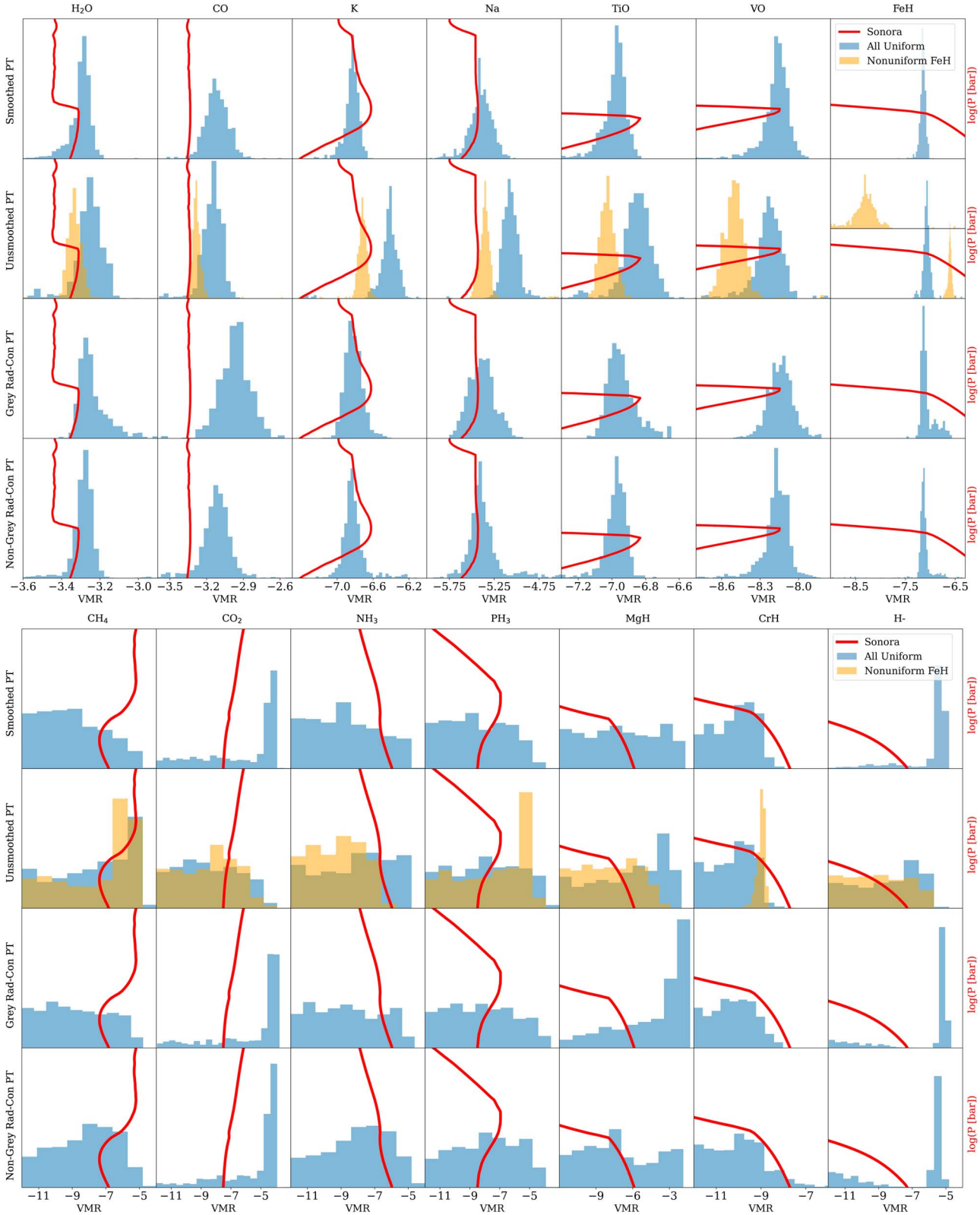

Figure 10. The posteriors of the fully uniform abundance parameters (blue) and the input self-consistent chemistry abundance profiles (red) for the four thermal profiles tested. Also shown are the posteriors for the nonuniform FeH retrieval (orange). The top plot shows constrained species and the bottom plot shows mostly unconstrained species. CrH is only constrained in the nonuniform FeH retrieval. Both the upper and lower abundance for the nonuniform FeH posterior are shown.

Appendix B
Nonuniform FeH Retrieval

This appendix contains information on the winning retrieval model. The model included an unsmoothed PT profile and a nonuniform FeH abundance profile. Figure 11 displays the corner plots of selected parameters and the 1σ retrieved spectra with residuals.

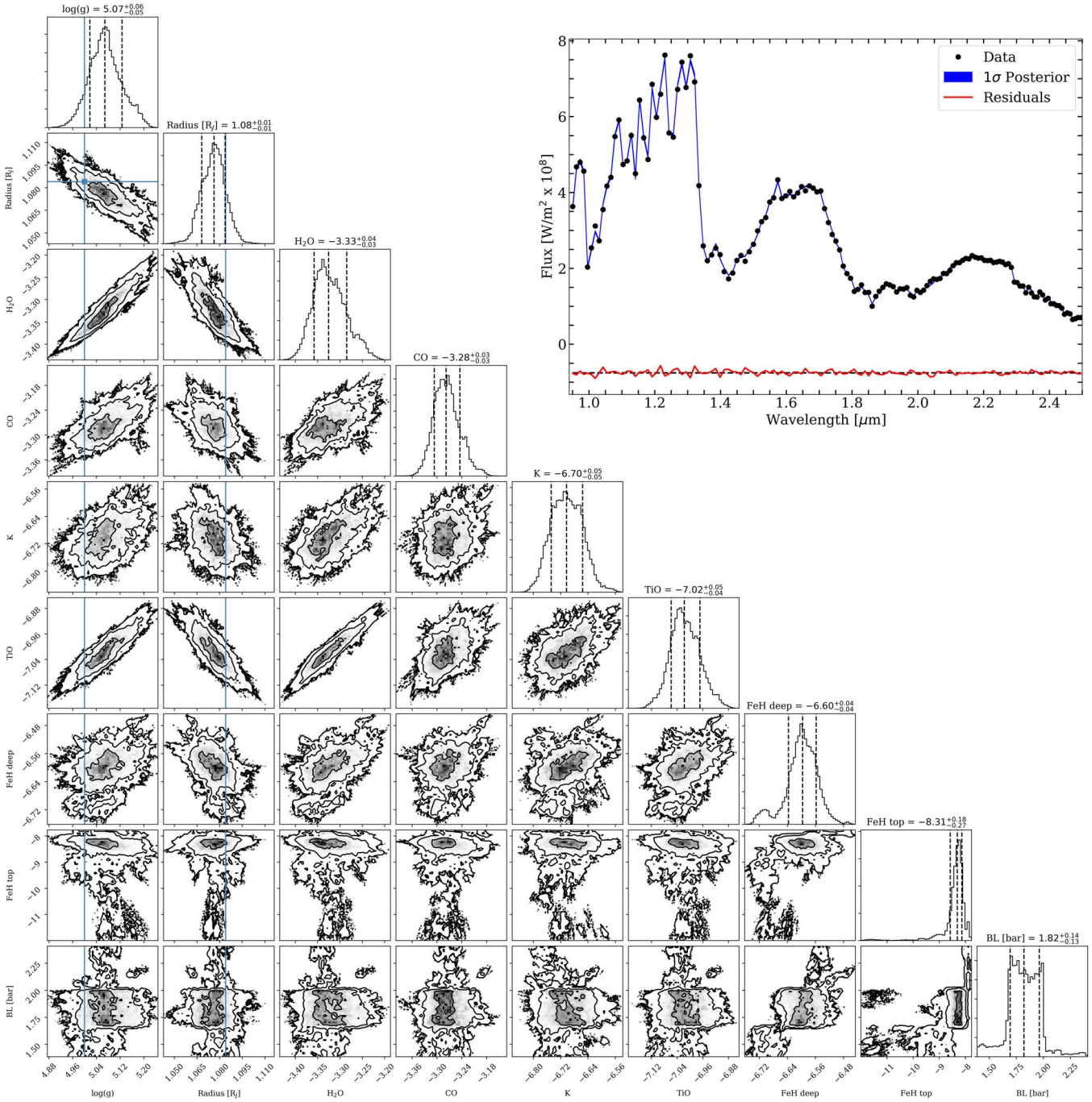

Figure 11. Corner plot of selected retrieved parameters including the six most abundant species for the nonuniform FeH retrieval. All abundances are log(VMR) values. The true values for surface gravity are indicated in blue. Upper figure is the 1σ retrieved spectra of the nonuniform FeH model with residuals.

Appendix C
Effects of Gases on L2 NIR SpeX Spectra

Figure 12 in this appendix displays synthetic SpeX observations of a cloud-free L dwarf derived from Sonora Bobcat models. Abundances of each gas were varied to highlight the location and magnitude of spectral impact of the gas on SpeX observations.

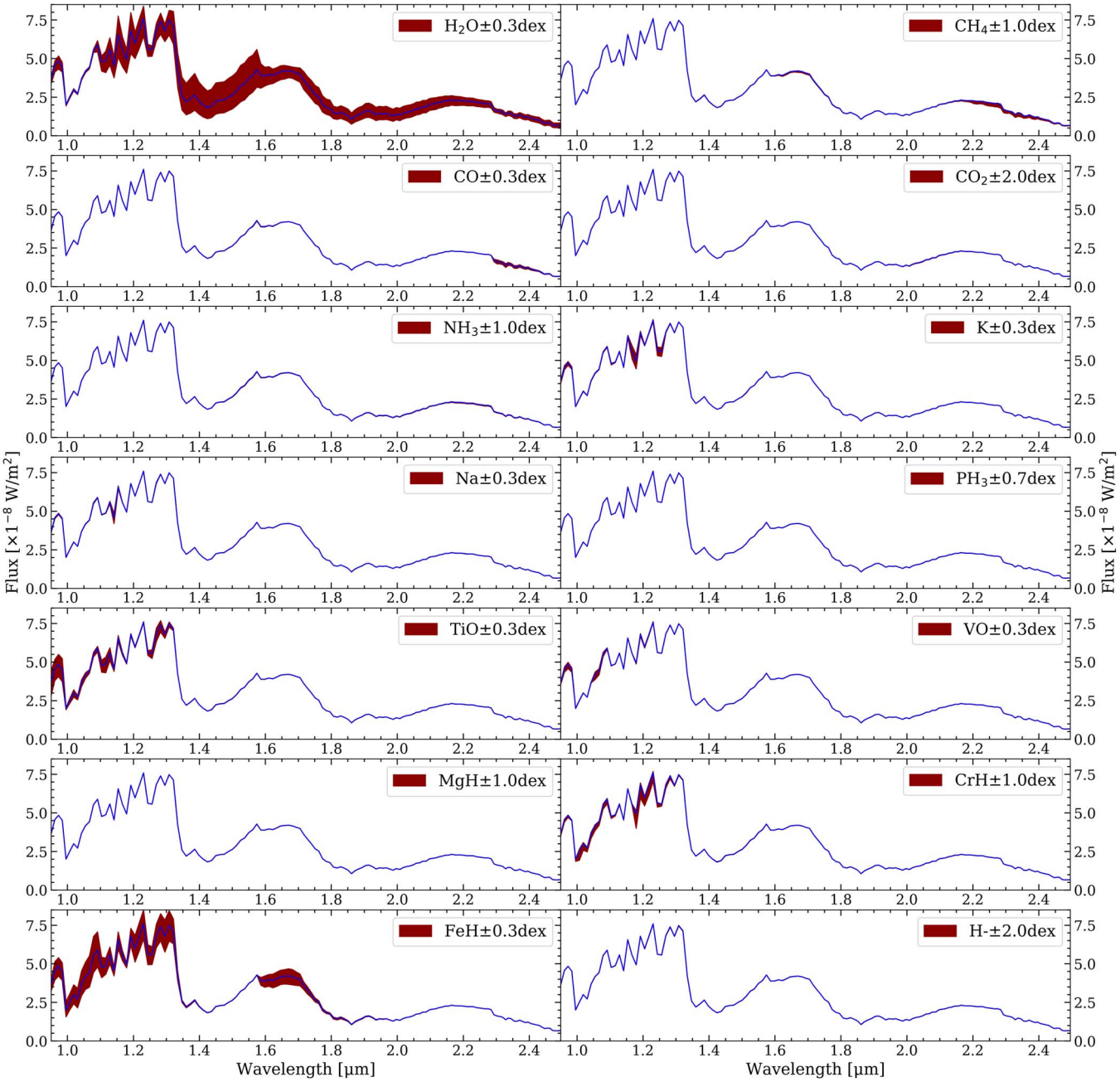

Figure 12. CHIMERA forward models using the Sonora *PT* profile and abundance profiles (blue) and the effect of changing each gas abundance profile ±X dex according to an allowable amount based on solar maximum. A dex of ±1.0 changes the abundance by 10× the Sonora value and shifts the abundance profile by 1 in log(VMR) space. The resulting spectra are not self-consistent.

ORCID iDs

Melanie J. Rowland https://orcid.org/0000-0003-4225-6314
Caroline V. Morley https://orcid.org/0000-0002-4404-0456
Michael R. Line https://orcid.org/0000-0002-2338-476X

References

Ackerman, A. S., & Marley, M. S. 2001, ApJ, 556, 872
Allard, F., Hauschildt, P. H., & Schwenke, D. 2000, ApJ, 540, 1005
Barber, R. J., Tennyson, J., Harris, G. J., & Tolchenov, R. N. 2006, MNRAS, 368, 1087
Bourrier, V., Kitzmann, D., Kuntzer, T., et al. 2020, A&A, 637, A36
Burgasser, A. J. 2014, in Astronomical Society of India Conf. Ser. 11, Int. Workshop on Stellar Spectral Libraries, 7
Burningham, B., Faherty, J. K., Gonzales, E. C., et al. 2021, MNRAS, 506, 1944
Burningham, B., Marley, M. S., Line, M. R., et al. 2017, MNRAS, 470, 1177
Burrows, A., Hubbard, W. B., Lunine, J. I., & Liebert, J. 2001, RvMP, 73, 719
Burrows, A., Hubbard, W. B., Saumon, D., & Lunine, J. I. 1993, ApJ, 406, 158
Burrows, A., Ram, R. S., Bernath, P., Sharp, C. M., & Milsom, J. A. 2002, ApJ, 577, 986
Chandrasekhar, S. 1935, MNRAS, 96, 21
Changeat, Q., Edwards, B., Waldmann, I. P., & Tinetti, G. 2019, ApJ, 886, 39
Cushing, M. C., Marley, M. S., Saumon, D., et al. 2008, ApJ, 678, 1372
Dulick, M., Bauschlicher, C. W., Burrows, J., et al. 2003, ApJ, 594, 651
Foreman-Mackey, D. 2016, JOSS, 1, 24
Foreman-Mackey, D., Hogg, D. W., Lang, D., & Goodman, J. 2013, PASP, 125, 306
Gravity Collaboration, Nowak, M., Lacour, S., et al. 2020, A&A, 633, A110
Gonzales, E. C., Burningham, B., Faherty, J. K., et al. 2021, ApJ, 923, 19
Gonzales, E. C., Burningham, B., Faherty, J. K., et al. 2022, ApJ, 938, 56
Guillot, T. 2010, A&A, 520, A27
Hargreaves, R. J., Hinkle, K. H., Bauschlicher, C. W., Jr., et al. 2010, AJ, 140, 919
Huang, X., Gamache, R. R., Freedman, R. S., Schwenke, D. W., & Lee, T. J. 2014, JQSRT, 147, 134
Kass, R. E., & Raftery, A. E. 1995, J. Am. Stat. Assoc., 90, 773
Kitzmann, D., Heng, K., Oreshenko, M., et al. 2020, ApJ, 890, 174
Lacis, A. A., & Oinas, V. 1991, JGR, 96, 9027
Lacy, B., & Burrows, A. 2023, ApJ, in press
Li, G., Gordon, I. E., Rothman, L. S., et al. 2015, ApJS, 216, 15
Line, M. R., Marley, M. S., Liu, M. C., et al. 2017, ApJ, 848, 83
Line, M. R., Teske, J., Burningham, B., Fortney, J. J., & Marley, M. S. 2015, ApJ, 807, 183
Line, M. R., Wolf, A. S., Zhang, X., et al. 2013, ApJ, 775, 137
Lodders, K. 1999, ApJ, 519, 793
Lodders, K., & Fegley, B. 2002, Icar, 155, 393
Lueber, A., Kitzmann, D., Bowler, B. P., Burgasser, A. J., & Heng, K. 2022, ApJ, 930, 136
Madhusudhan, N., Amin, M. A., & Kennedy, G. M. 2014, ApJL, 794 L12
Madhusudhan, N., Bitsch, B., Johansen, A., & Eriksson, L. 2017, MNRAS, 469, 4102
Madhusudhan, N., & Seager, S. 2009, ApJ, 707, 24
Marley, M. S., & Robinson, T. D. 2015, ARA&A, 53, 279
Marley, M. S., Saumon, D., Guillot, T., et al. 1996, Sci, 272, 1919
Marley, M. S., Saumon, D., Visscher, C., et al. 2021, ApJ, 920, 85
McKemmish, L. K., Yurchenko, S. N., & Tennyson, J. 2016, MNRAS, 463, 771
Mollière, P., Stolker, T., Lacour, S., et al. 2020, A&A, 640, A131
Mukherjee, S., Fortney, J. J., Batalha, N. E., et al. 2022, ApJ, 938, 107
Öberg, K. I., Murray-Clay, R., & Bergin, E. A. 2011, ApJL, 743, L16
Parmentier, V., & Guillot, T. 2014, A&A, 562, A133
Phillips, M. W., Tremblin, P., Baraffe, I., et al. 2020, A&A, 637, A38
Robinson, T. D., & Catling, D. C. 2012, ApJ, 757, 104
Rothman, L. S., Gordon, I. E., Barber, R. J., et al. 2010, JQSRT, 111, 2139
Saumon, D., & Marley, M. S. 2008, ApJ, 689, 1327
Schwenke, D. W. 1998, FaDi, 109, 321
Sousa-Silva, C., Al-Refaie, A. F., Tennyson, J., & Yurchenko, S. N. 2015, MNRAS, 446, 2337
Stock, J. W., Kitzmann, D., Patzer, A. B. C., & Sedlmayr, E. 2018, MNRAS, 479, 865
Tennyson, J., & Yurchenko, S. 2018, Atoms, 6, 26
Tennyson, J., & Yurchenko, S. N. 2012, MNRAS, 425, 21
Tremblin, P., Amundsen, D. S., Chabrier, G., et al. 2016, ApJL, 817, L19
Weck, P. F., Schweitzer, A., Stancil, P. C., Hauschildt, P. H., & Kirby, K. 2003, ApJ, 582, 1059
Yurchenko, S. N., Barber, R. J., & Tennyson, J. 2011, MNRAS, 413, 1828
Yurchenko, S. N., & Tennyson, J. 2014, MNRAS, 440, 1649
Yurchenko, S. N., Tennyson, J., Barber, R. J., & Thiel, W. 2013, JMoSp, 291, 69
Zalesky, J. A., Line, M. R., Schneider, A. C., & Patience, J. 2019, ApJ, 877, 24
Zalesky, J. A., Saboi, K., Line, M. R., et al. 2022, ApJ, 936, 44
Zhang, Y., Snellen, I. A. G., Bohn, A. J., et al. 2021, Natur, 595, 370